Controlled formation of Ag-Ag_xO nanoparticles on the surface of commercial TiO_2 based composites for enhanced photocatalytic degradation of oxalic acid and phenol

Zsejke-Réka Tóth (Writing - original draft) (Writing - review and editing) (Validation) (Methodology) (Conceptualization), Klara Hernadi (Supervision) (Funding acquisition), Lucian Baia (Supervision) (Funding acquisition), Gábor Kovács (Writing - original draft) (Writing - review and editing) (Methodology) (Investigation), Zsolt Pap (Supervision) (Investigation) (Conceptualization)

PII: S0920-5861(20)30437-5

DOI: https://doi.org/10.1016/j.cattod.2020.06.051

Reference: CATTOD 12969

To appear in: *Catalysis Today*

Received Date: 1 October 2019

Revised Date: 16 May 2020

Accepted Date: 13 June 2020

Please cite this article as: Tóth Z-Réka, Hernadi K, Baia L, Kovács G, Pap Z, Controlled formation of Ag-Ag_xO nanoparticles on the surface of commercial TiO_2 based composites for enhanced photocatalytic degradation of oxalic acid and phenol, *Catalysis Today* (2020), doi: https://doi.org/10.1016/j.cattod.2020.06.051

Controlled formation of Ag-Ag_xO nanoparticles on the surface of commercial TiO_2 based composites for enhanced photocatalytic degradation of oxalic acid and phenol

Zsejke-Réka Tóth[a, b], Klara Hernadi[a], Lucian Baia[b, c], Gábor Kovács[b, d,*], Zsolt Pap[b, d,*]

[a]Faculty of Science and Informatics, Department of Applied and Environmental Chemistry, University of Szeged, Rerrich Béla tér 1, HU-6720, Szeged, Hungary

[b]Nanostructured Materials and Bio-Nano-Interfaces Center, Interdisciplinary Research Institute on Bio-Nano-Sciences, Babeș-Bolyai University, Treboniu Laurian 42, RO-400271, Cluj-Napoca, Romania

[c]Faculty of Physics, Babeș-Bolyai University, M. Kogălniceanu 1, RO-400084, Cluj-Napoca, Romania

[d]Institute of Environmental Science and Technology, University of Szeged, Tisza Lajos krt. 103, HU-6720, Szeged, Hungary

*-Corresponding authors

* e-mail addresses: pzsolt@chem.u-szeged.hu, pap.zsolt@phys.ubbcluj.ro (Zs. P.), k.gabor84@chem.u-szeged.hu, gkovacs@chem.ubbcluj.ro (G. K.)

Graphical abstract

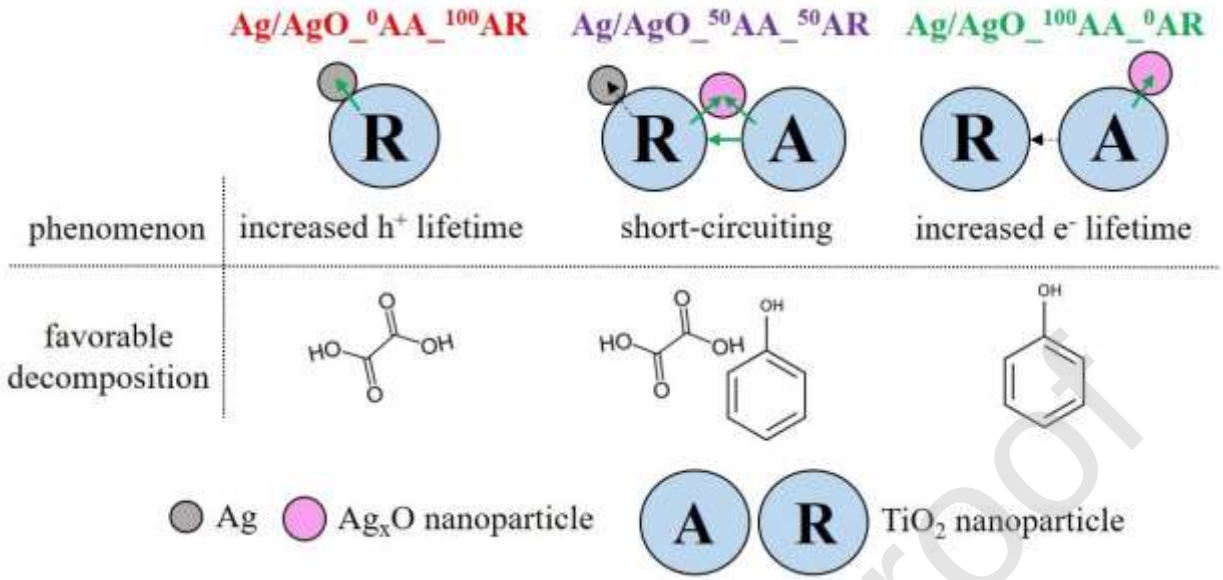

Research highlights:

1. The rutile crystal phases are responsible for the formation of silver nanoparticle.
2. The Ag nanoparticles can be transformed into Ag_xO.
3. The Ag/Ag_xO nanoparticles have positive effect on the titania activity.
4. The Ag/Ag_xO nanoparticles are playing the role of a charge separator.

Abstract:

The issues regarding the low stability of the Ag nanoparticles during the photodegradation processes are already well-known, being easily transformed to Ag_xO. On the other hand, the (photo)catalytic efficiency of TiO_2 can be increased by modifying its surface with noble metal nanoparticles. Therefore, the present work focused on commercial TiO_2 *(Aldrich anatase and rutile)* mixtures with well-defined ratios, applying Ag nanoparticles on the surface of the titania with or without using a reducing agent. The transformation of the Ag nanoparticles into AgO was monitored in the frame of the anatase and rutile content, while the transformation's effect on the photocatalytic activity was examined (degradation phenol and oxalic acid under UV). It was concluded that the Ag nanoparticles deposited on the surface of rutile can increase the efficiency of charge

separation while, present on the surface of the anatase, the formed amorphous AgO nanoparticles are behaving similarly. The tertiary and quaternary composites generally had higher photocatalytic efficiencies toward oxalic acid, than the corresponding commercial TiO_2 mixtures. The low stability of the Ag nanoparticles was also found in our investigations, as the NPs are transformed into Ag_2O, which can be re-transformed during the photocatalytic processes to Ag. On the other hand, the stability of the AgO is not affected during the aging period. Therefore, it can be assumed, that AgO is more stable on the surface of the anatase phase of the titania than the Ag and the Ag_2O nanoparticles.

Keywords: quaternary composites; Ag nanoparticles; electron transfer; photocatalysis

1. Introduction

One of our most emerging problems is the decreasing availability of clean, accessible, and potable water sources. Nowadays, different filtration methods (e.g., regular, membrane, coagulation, flocculation, sedimentation, and distillation) are widely used for water purification [1]. These methods of purification are used for removing chemicals and biological contaminants. However, in some of the cases, they are insufficient to keep pace with the new challenges given by new classes of pollutants, such as persistent pharmaceuticals (e.g., antibiotics, antipyretics substances, etc.), organic dyes and other contaminants. Therefore, in order to solve both problems, we need to develop a method toward unique industrial needs that is low-cost, non-toxic, and highly efficient.

In the early ’70s, the research with photoelectrolysis [2] started to focus on using TiO_2 for water splitting and photoelectrocatalytic H_2 evolution. The main problem with TiO_2 is that it can be excited mostly with UV light [3]. In order to enlarge its applicability spectra toward visible light and a more significant number of organic contaminants, investigations were concentrated on modifying the structure of titania [4, 5].

A widely researched approach in order to overcome these issues were to modify the band gap/excitation energy of TiO_2 by modifying with non-metallic elements (N [6], S [7], P [8], rGO [9] etc.), or depositing noble metals on the surface of the semiconductor (Ag [10], Au [11], and Pt [12]) which can increase the efficiency of the separation charge carriers [13]. Additionally, noble metals can help the adsorption of some organic compounds on the surface of titania (e.g., methyl orange), increasing in this way, the photocatalytic efficiency of the semiconductor [14]. Moreover, attempts were made using composites containing two semiconductor oxides [15, 16] and with non-Ti based semiconductor oxides (ZnO [17], Cu_xO [18], Ag_xO [19, 20], In_2O_3 [21]).

Among other well-known Ag-based materials (e.g. Ag_xS [22], AgX [23, 24], Ag_3PO_4 [25]), Ag_xO based materials (AgO, Ag_2O) are considered to be promising alternatives in photoactive applications. Although, the bottle-neck of these semiconductors it that their strong photosensitivity is often “combined” with low operational stability under irradiation with visible/UV light [26], in parallel with the non-controlled formation of Ag nanoparticles on the surface of the silver (I) oxide [27]. On the other hand, the stability of the Ag_2O can be increased by deposition of silver nanoparticles with *in situ* method, generated under light irradiation [20]. However, it is challenging that Ag_2O is transformed into/covered by Ag nanoparticles, usually losing in this way its photocatalytic efficiency. Other semiconductors

were used for promoting the stability of the material, such as Ag_2O/AgI [28], Ag_2O/TiO_2 [29], Ag_2O/C_3N_4 [30].

The Ag_2O/TiO_2 composites were investigated in several photocatalytic processes because Ag_2O has relatively low band gap energy and usually has facile preparation pathways [31]. The Ag_2O/TiO_2 composites are p-n type semiconductors, where the band gap energy of Ag_2O is ≈1.3 eV [32], while this value is 3.2 eV for anatase [33] and 3.0 eV in the case of rutile [34]. The increasing interest toward p-n type semiconductors can be attributed to their improved e-h^+ charge separating properties [34]. Moreover, if Ag nanoparticles are deposited onto the surface of the composites, it can be beneficial for the electron transfer between the TiO_2 and Ag_2O, increasing the photocatalytic efficiency of the composites [31].

Besides the electron trap property of silver nanoparticle, it also could be distinguished from the surface plasmon resonance effect of the Ag [35], which helps the excitation of the electrons on the surface and have a new absorption band in the visible region [36]. In Ag/TiO_2 composites could be formed the Schottky barrier, which appeared at Ag and TiO_2 contact region. This barrier also helps with increasing TiO_2 activity [37].

According to Wei *et al.* [38], Ag nanoparticles can be spontaneously transformed to Ag_2O on the surface of anatase. However, Ag_2O undergoes a disproportionation reaction, forming Ag and AgO nanoparticles, although the latter ones are unstable at room temperature [18]. L. Gomathi Devi *et al.* claimed that the deposition of Ag nanoparticles on the surface of titania could also help the electron transfer between the anatase and rutile, as the electron from the valance band of anatase could be promoted to the valence band of the rutile [39].

Taking into account the aspects mentioned above, in the present work, Ag nanoparticles were deposited with or without reduction onto the surface of different commercial TiO_2 (*Aldrich anatase (AA) and rutile (AR))* mixtures. The amount of the transformed Ag_xO was analyzed by using several investigation methods, taking under the loupe the synergic effect of Ag/Ag_xO on the activity of TiO_2. The novelty of this work consists of an in-detail investigation on how different crystal phases of the TiO_2 can affect the deposition of Ag nanoparticles, as it was found that Ag nanoparticles were formed on the rutile crystal phase and AgO nanoparticles have formed by using anatase crystal phase.

2. Material and methods

2.1. Chemicals

All chemicals were used without any further purification. Commercial *Aldrich anatase* (99.8 %, trace metal basis) and *Aldrich rutile* (99.9 %, trace metal basis), were purchased

from Sigma-Aldrich (Steinheim, Germany). Trisodium citrate ($Na_3C_6H_5O_7$, 99.0%, Chempur, Poland); silver-nitrate ($AgNO_3$, 99.8 %, Penta industry, Romania); sodium borohydride ($NaBH_4$, 96 %, Merck, Germany) were used for the synthesis of Ag/Ag_xO nanoparticles. Sodium chloride (analytical reagent) was purchased from Molar Chemicals, Hungary (99.9%).

2.2. Synthesis of the TiO_2 mixtures by mechanical mixing

Mechanical mixing in an agate mortar was applied for 2×5 min to obtain the mixtures of commercial titania. Well defined ratio of commercial *Aldrich anatase* (AA) and *Aldrich rutile* (AR) were mixed to obtain the following composites: AA:AR= 0:100, 10:90, 25:75, 50:50, 75:25, 90:10 and 100:0. The obtained composites were named $^{x}AA\_^{y}AR$, where x and y represent the ratio of the component in the mixture.

2.3. Synthesis of the $Ag/AgO/TiO_2$ composites

Our previously described method was adapted for the synthesis of silver nanoparticles [40]. Briefly, 500 mg of commercial TiO_2 (AA and/or AR) powder was added directly into the reaction vessel with 130 mL of distilled water and ultrasonicated for 15 minutes. Afterward, 18.9 mL (0.63 mM) trisodium citrate was added to the suspension, followed by 30 minutes of stirring. In the next step, 1.65 mL (22.8 mM) of $AgNO_3$ was added in the suspension, in order to obtain a concentration of 0.8 % of Ag/Ag_xO on the surface of TiO_2. Finally, two different experimental approaches were followed:

(i) reduction without a reducing agent (wo/$NaBH_4$): after stirring for 30 minutes, the color of the suspension changed from white to greyish (Fig. 1), while the intensity of the color depended on the amount of the AR. Finally, 5 g of NaCl was added, followed by a washing step with 2×50 mL H_2O at 6000 RPM. The abbreviation of the as-synthesized materials will be as follows $Ag/AgO\_^{x}AA\_^{y}AR\_woNaBH_4$;

(ii) by using $NaBH_4$, as reducing agent: after 30 minutes of stirring, the color change was the same but followed by the addition of 3 mL of $NaBH_4$ (0.15 M) to the mixture. After stirring for another 1 hour, the same washing process was used as described above. The used abbreviation for these samples will be $Ag/AgO\_^{x}AA\_^{y}AR$. In both cases, sodium chloride was added to increase the sedimentation rate of the suspension.

2.4. Characterization methods and instrumentation

JASCO-V650 diffuse reflectance spectrophotometer (DRS) with an integration sphere **ILV-724** (the spectra of the samples were recorded between 250-800 nm) was used for investigation of the optical properties of the composites. DRS was used to demonstrate the influence of Ag/Ag_xO on the band gap energy values of TiO_2. The indirect band gap energy values of the materials were estimated by using the Tauc plot [41], while the first derivative spectrum ($dR/ d\lambda$) was also obtained and analyzed. In the presence of Ag/Ag_xO, the DRS was used for the detection of the plasmonic band, specific for both nanoparticles [42]. The DRS was also used to demonstrating the stability of the Ag/TiO_2 composites (measuring the differences after the synthesis, after 6 months of aging and after the photodegradation process(es)).

XPS measurements were performed on a SPECS PHOIBOS 150 MCD instrument to clarify the oxidation state of silver, with monochromatized Al K_α radiation (1486.69 eV) at 14 kV and 20 mA, and pressure lower than 10^{-9} mbar. Samples were mounted on the sample holder using double-sided adhesive carbon tape. High-resolution Ag 3d spectra were recorded in steps of 0.05 eV. The analysis of the obtained data was carried out with CasaXPS software. All peaks have been deconvoluted using Shirley background and Lorentzian-Gaussian line shapes. The applied value of the Gaussian-Lorentzian ratio was 90. A series containing four samples were analyzed, namely Ag/AgO-^{100}AA_^{0}AR, Ag/AgO-^{75}AA_^{25}AR, Ag/AgO-^{50}AA_^{50}AR and Ag/AgO-^{0}AA_^{100}AR, respectively.

Rigaku Miniflex II X-ray diffractometer (XRD) ($\lambda_{CuK\alpha}$ = 0.15406 nm, 40 kV, 30 mA, between 43°–49° (2θ°) with 0.3 (2θ°)·min^{-1} scanning speed) was used for the investigation of catalysts structure.

FEI Technai G2 20 X-TWIN transmission electron microscope (TEM), operating at an accelerating voltage of 200 kV was used for the demonstration of the deposited nanoparticles on the TiO_2.

Fluorescence measurements were recorded using a **Jasco LP-6500 spectrofluorometer** with a 1 nm spectral resolution, equipped with a Xenon lamp as an excitation source, coupled to an epifluorescence accessory (EFA 383 module). Fluorescence spectra were collected in the wavelength range of 350-600 nm using a fixed excitation wavelength at 325 nm, bandwidths of 5 nm were employed in both excitation and emission.

2.5. Photocatalytic investigations

The investigations of photocatalytic activities were carried out under irradiation of UV light (6 × 6 W, λ_{max}= 365 nm), within a double-walled photoreactor (100 mL), which was

surrounded by a thermostat jacket (25 °C). The concentration of the suspension was 1 $g \cdot L^{-1}$, which was continuously stirred, and air supply was assured with an airflow of ≈ 1 L · min. The same photocatalytic reaction setup was also used for the investigation of efficiencies under irradiation with visible light, except that the reactor was thermostated by 1 M $NaNO_2$ solution (for eliminating any UV photons) and irradiated by 4×24 W (DÜVI 25920/R7S, Hungary, λ_{max} = 545 nm). The sampling in the first hour was taken every 10 minutes, and in the second hour by 20 minutes. The changes of the concentration of the model pollutant (0.5 mM of phenol and 5 mM of oxalic acid) were measured by **Merck-Hitachi L-7100** with low-pressure gradient pump, equipped with a **Merck-Hitachi L-4250** UV-Vis detector and a **Lichrospher Rp 18** column applying methanol/water mixture and H_2SO_4 as eluent using 210 nm (phenol) and 206 nm (oxalic acid) as the detection wavelength.

Recycling tests were used for the stability of the catalyst investigation. After the degradation test, the catalyst was washed with 3 × 50 mL of H_2O for 10 min at 4400 RPM and dried for 12 hours at 40 ºC and it was re-used in the same conditions (except that the sampling was changed to intervals of 30 minutes intervals).

3.Results and discussion

3.1 Preparation and characterization of the samples

The first observation during the synthesis of the samples was that with the addition of trisodium citrate into the suspension of TiO_2 (Fig. 1a), no color change was observed. On the other hand, by adding $AgNO_3$ (Fig. 1b), the color has changed to grey, and the intensity increased with the amount of rutile in the sample, which is probably due to Ag^0 deposition onto the surface of TiO_2. In the case Ag/AgO-^{x}AA_^{y}AR_woNaBH$_4$, by adding sodium chloride into the suspension, its color has changed from grey to creamy pink (Fig. 1c). The intensity of the color change depended, similar to the previous case, on the amount of rutile. When $NaBH_4$ was added as a reducing agent (Ag/AgO-^{x}AA_^{y}AR), the color of the suspension changed to dark cream (brownish, wood color), then to a brighter nuance after the addition of NaCl (Fig. 1d).

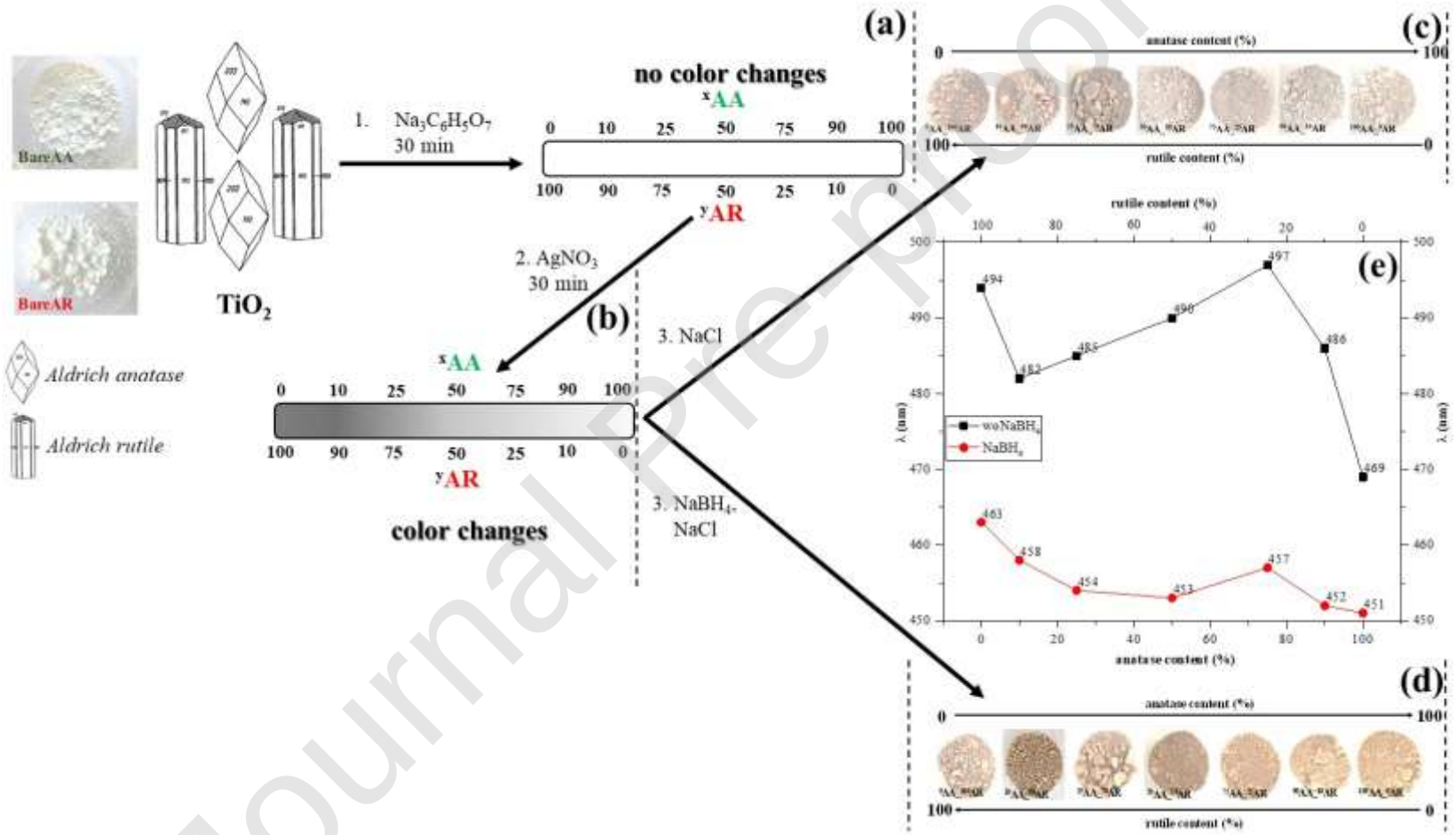

Figure 1. The color change sequence of the samples: (a) the color of the catalyst did not change during the first step; (b) after adding the noble metal precursor to the suspension, it turned to grey (which became brighter with an increase in the amount of anatase); color effect of Ag nanoparticles deposition (c) without (Ag/AgO-^{x}AA_^{y}AR_woNaBH$_4$) - and (d) using a reducing agent (Ag/AgO-^{x}AA_^{y}AR) on the surface of the commercial TiO_2; (e) the position plasmonic bands of Ag-based composites.

The typical plasmonic resonance band of the isolated Ag nanoparticles (≈10-20 nm) can be observed at ≈400 nm [42-44]. If the Ag nanoparticles increase in size to tens of nanometers or aggregates of Ag nanoparticles are formed, or even non-spherical nanoparticles are present, the absorption band can appear at longer wavelengths [43, 44]. As Fig. 1e shows, the plasmonic resonance bands of the materials are located between 451-494 nm.

Two different regions can be separated:

(i) using $NaBH_4$ (Ag/AgO-^{x}AA_^{y}AR), as a reducing agent, the observed plasmonic resonance bands were located between 451-463 nm, where the silver specific plasmonic resonance band showed a large redshift. According to Feng *et al.* [45], this shift could be attributed to the high refraction index of TiO_2. In this case, we can conclude that the resulted plasmonic resonance bands have linear trend within a single exception: Ag/AgO-^{75}AA_^{25}AR;

(ii) when no reducing agent was used (Ag/AgO-^{x}AA_^{y}AR_woNaBH$_4$), the obtained plasmonic resonance bands were located between 469-494 nm, which can be attributed to agglomerated Ag nanoparticles or transformation into other materials. In this case, an outstanding value was obtained for the sample Ag/AgO-^{75}AA_^{25}AR_woNaBH$_4$. Before reaching this specific value, the plasmonic resonance bands suffer a redshift (the plasmonic band maxima being located at higher wavelengths with the increase of the amount of the anatase), while after Ag/AgO-^{75}AA_^{25}AR_woNaBH$_4$, the samples are giving blueshift.

X-ray diffractometry was used for the confirmation of the crystal phase mixture of commercial TiO_2 and any possible changes during the synthesis/deposition processes. JCPDS 21-1272 (*anatase)* and JCPDS 21-1276 (*rutile)* cards were used for the correct identification of two different crystal phases, from which we can conclude that none of the titania is suffering any structural changes during the synthesis (Fig. S1, Fig. 2). The specific diffraction peaks of AgO (JCPDS 84-1108) and Ag_2O (JCPDS-75-1532) were not found because (i) the applied amount of these materials was low (only 0.8 % wt.%) or (ii) the obtained values are below the threshold limit of the approach/setup.

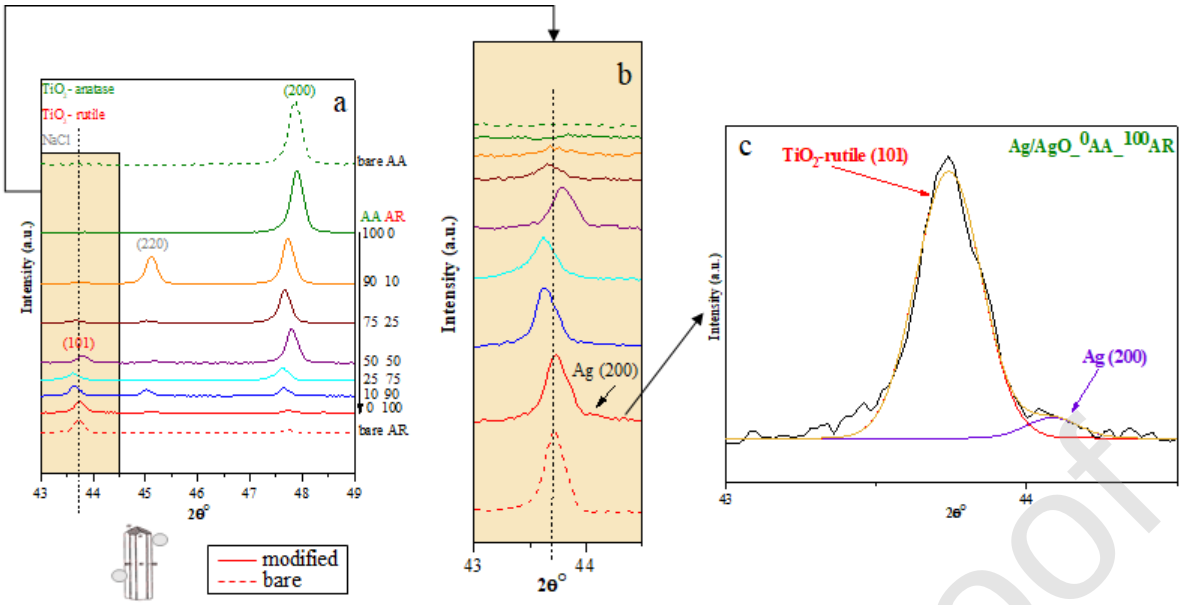

Figure 2. X-ray diffractograms of the samples prepared using a reducing agent: (a) complete patterns of samples, (b) enlarged pattern and (c) deconvolution of the pattern of Ag/AgO-^{0}AA_^{100}AR.

On the other hand, the specific reflection of silver nanoparticles (JCPDS 04-0783; (200), at 44.0°) generally can overlap the specific reflection of (101) Miller indexed rutile. As can be observed in Fig. 2a, by deconvolution of Ag/Ag$_x$O-^{00}AA_^{100}AR, the specific reflection of silver nanoparticles appears. As the amount of rutile decreased in the samples, the intensity of the Ag signal decreased as well (Fig. 2b), until disappearing entirely in the case of the sample Ag/AgO-^{100}AA_^{0}AR (Fig. 2). Briefly, we can conclude that the rutile crystal phase is responsible for Ag nanoparticles' formation because the typical reflection for Ag nanoparticles are present and changed together with the signal of rutile [46]. Since the specific plasmonic resonance bands were present in all samples (Fig. 1), we can suppose that Ag was transformed to Ag$_x$O, which can appear in an amorphous phase (being not observable in XRD pattern shown in Fig. 2). The transformation of silver to Ag$_x$O is also supported by the fact that no silver leaching was observed during the synthesis as the supernatant was transparent.

Transmission electron microscopy was used to measure the size shape of the nanoparticles. The commercial TiO_2 crystals had particle sizes between 80-100 nm (Aldrich anatase, Fig. 3e-f) and 100-150 nm (Aldrich rutile, Fig. 3a-b). In the case of Ag/AgO-^{0}AA_^{100}AR, 5-10 nm sized particles were obtained (Fig. 3b). Since, in the XRD patterns (Fig.

2), only Ag-specific diffraction peaks were observed. Therefore, we can suppose that the observed particles on the surface of titania are indeed silver nanoparticles. Our previous work also supported this statement [38] as we showed that the preferred forming of Ag nanoparticles was observed when rutile was used (also described by Quesada-Cabrera *et al*. [44]).

Moreover, in the case of Ag/AgO-^{100}AA_^{0}AR, larger Ag-based nanoparticles were also found (15-20 nm). However, in the case of Ag/AgO-^{50}AA_^{50}AR, both particle size values were observed (Fig. 3c and 3d). The obtained larger particles could be assigned as (i) agglomerated silver nanoparticles [44] or (ii) Ag_xO [36, 38]. Since, as shown in Fig. 3, there is no any sign of agglomerated metal nanoparticles and the sample Ag/AgO-^{100}AA_^{0}AR shows a lower value of plasmonic resonance band position (451 nm, Fig. 1e), therefore we can suppose that Ag_xO was formed. In order to elucidate this hypothesis, results of XPS investigations are discussed in later sections of the paper.

As it is shown in Fig. 4a, the as-synthesized metal-based nanoparticles can influence the light absorption capacity of TiO_2. As it was predictable from the literature, the calculated values for the indirect band gap energy (E_g) were between 2.97-3.18 eV (Fig. 4b) for the bare catalysts (^{x}AA_^{y}AR). However, it is also not surprising that by noble metal deposition (Ag/AgO-^{x}AA_^{y}AR) on the surface of titania, those values shifted to the visible light range (Fig. 4b). Without any reducing agent (Ag/AgO-^{x}AA_^{y}AR_woNaBH$_4$), the obtained values are closer to the values of the titania mixtures. Therefore, we focused on the composites, where Ag/Ag_xO nanoparticles were deposited by using the reducing agent. In the case of Ag/AgO-^{x}AA_^{y}AR only Ag/AgO-^{25}AA_^{75}AR (2.79 eV, Fig. 4b) resulted higher band gap energy value than the commercial catalysts (2.55 eV, Fig. 4b). In all other cases the modification of the composites was successful, moreover in the case of Ag/AgO-^{75}AA_^{25}AR sample resulted in 20 % (+0.53 eV) increasing of band-gap energy value (Ag/AgO-^{75}AA_^{25}AR-2.38 eV; ^{75}AA_^{25}AR-2.91 eV, Fig. 4b).

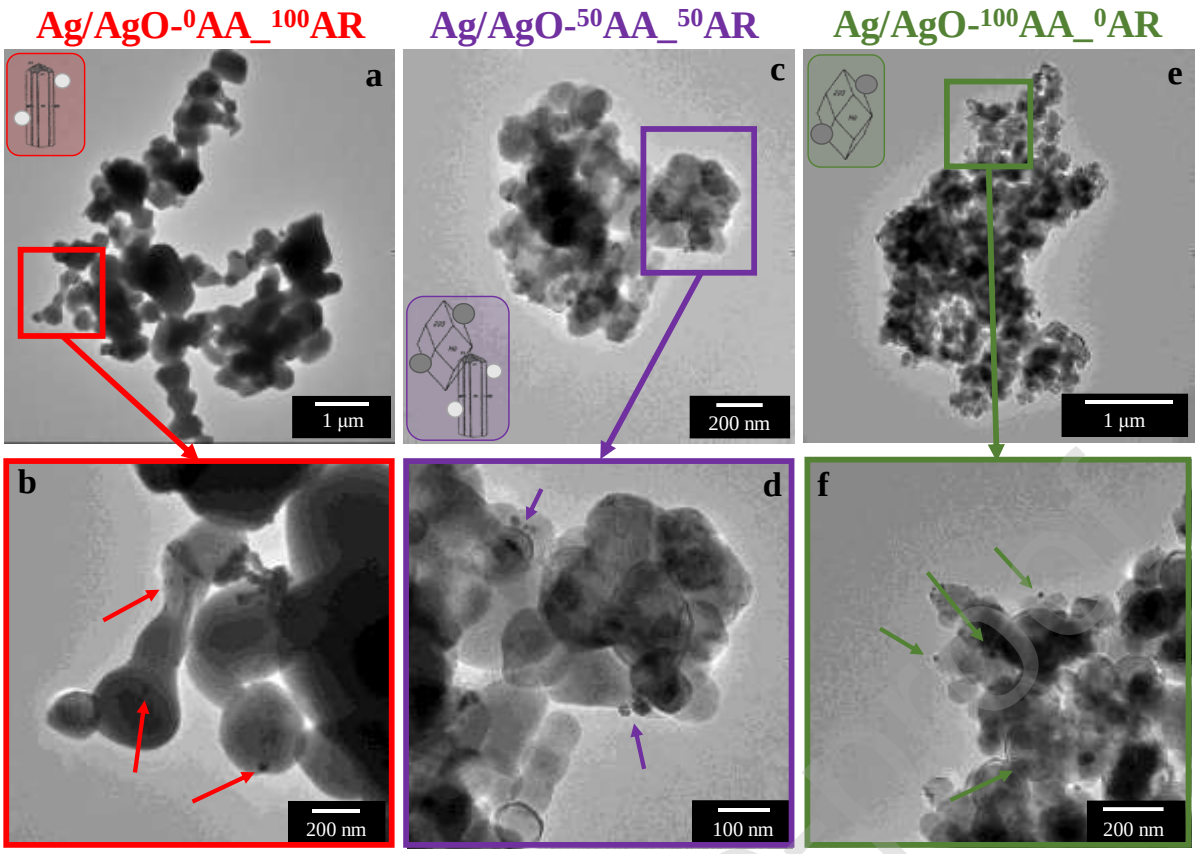

Figure 3. TEM micrographs of (a-b) Ag/AgO-^{0}AA_^{100}AR, (c-d) Ag/AgO-^{50}AA_^{50}AR and (e-f) Ag/AgO-^{100}AA_^{0}AR samples.

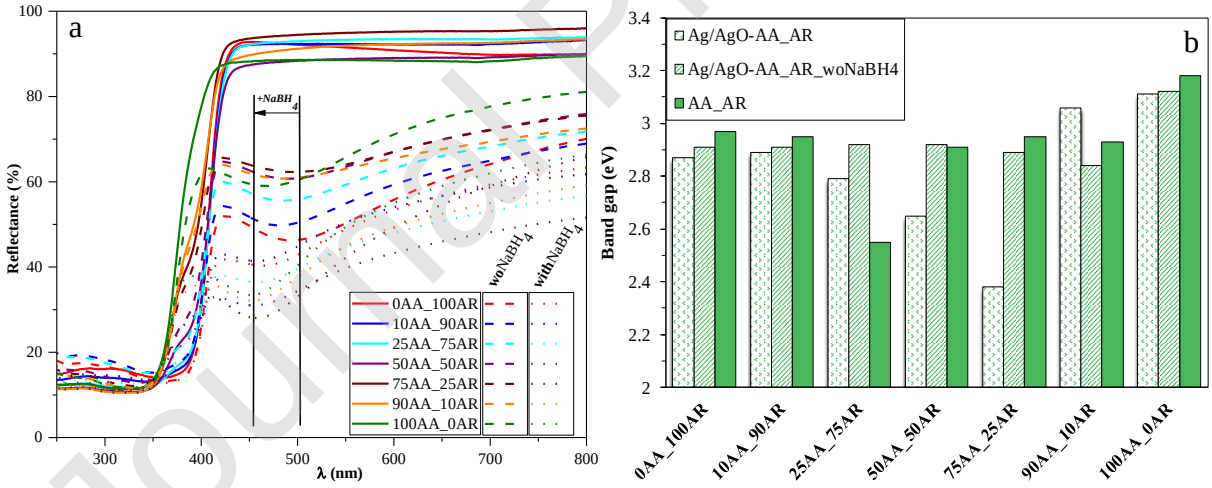

Figure 4. (a) diffuse reflectance spectroscopy of the samples; (b) band gap energy values of bare and modified TiO_2 catalysts.

As the ratio of titania-based crystal phases changed, two different light absorption capacities were detected (Fig. 4a), due to the presence of rutile and anatase, therefore the specific indirect band gap energy value cannot be clarified based on the two crystal phase-

specific band gap energy weighted average. The mixture of AA and AR showed a weighted average band gap value, and sometimes also lower values were obtained (Fig. 4). The reason for the lower band gap energy values can be attributed to the enhanced electron transfer between the two titania phases.

As it is shown in Fig. 5, by increasing the amount of the anatase in the case of ^{x}AA_^{y}AR samples resulted in a smaller increase in the first order derivative spectra – I_{AA}/I_{AR} value. Thus, that the light absorption of photostable rutile is more favored. Moreover, only in the cases of ^{100}AA_^{0}AR samples, the anatase dR/dλ peak is more intense than the rutile with a 2.94 AA/AR ratio value (Fig. 5). However, since the commercial Aldrich anatase contains a small amount of rutile an apparent ratio was noted, AA/AR ratio is not "infinite". If the light absorption would be "ideal", then the intensity ratio I_{AA}/I_{AR} should be the same as the weight ratio of AA and AR. In the case of the Ag/AgO-^{x}AA_^{y}AR sample series (red straight line), I_{AA}/I_{AR} ratio changed significantly in favor of anatase. In the case of the Ag/AgO-^{100}AA_^{0}AR sample, the intensity ratio value was 80 % higher than in the corresponding bare photocatalyst. The reduced electron transition band intensity value of rutile is due to fact that the metal nanoparticle accepts an electron from the conduction band of rutile. Consequently, the Ag metal nanoparticles should be located on the surface of rutile; otherwise, the electron transfer would not be possible.

In the cases of Ag/AgO-^{0}AA_^{100}AR and Ag/AgO-^{10}AA_^{90}AR samples, silver nanoparticles were detected by XRD (Fig. 2). If the character of the Ag nanoparticle did not change its structure, the AA/AR ratio increase would be linear. It was evident that the Ag nanoparticles changed their structure, characteristics and even transformed into other compounds during or after the deposition process because reaching the sample Ag/AgO-^{75}AA_^{25}AR, the intensity of the AA/AR ratio suddenly increases (Fig. 5). Because we have not found any sign of other crystal structures (Fig. 2), the newly formed silver-containing material may be amorphous. This is a somewhat plausible approach as Ag_xO can be obtained easily from Ag.

Based on the I_{AA}/I_{AR} from the first derivatives of DRS, we can conclude that the presence of anatase and rutile can control the ratio of the Ag/AgxO. While the amount of rutile is higher in samples, the obtained trend is linear. Reaching the ^{75}AA_^{25}AR, the trend changed suddenly due to the character change of the Ag nanoparticles.

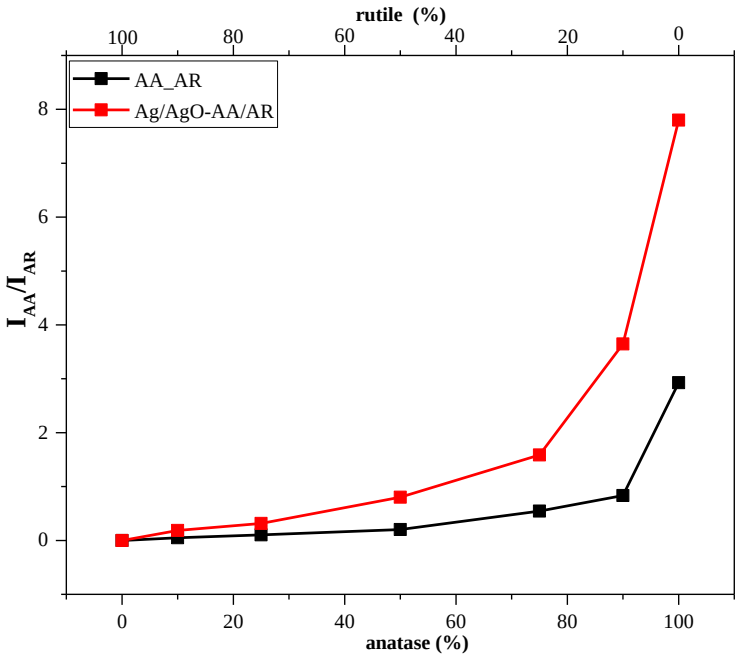

Figure 5. Ag/Ag_xO formation effect on the anatase and rutile electron transition band ratios obtained from the first order derivative of the DRS spectra.

Based on the other experimental approaches and facts provided until this point of the present manuscript, it was clear that several silver species can be present on the surface of our materials. It was also clearly demonstrated that by changing the anatase and rutile ratio within the composites, the ratio of the Ag species is changing as well. Hence, it was necessary to identify these species. Considering the experimental data available it was suspected that AgO formation was favored by the presence of anatase, while Ag by the presence of rutile, therefore, the samples' Ag3d XPS spectra were analyzed. In the case of sample Ag/AgO-^{100}AA_^{0}AR both under the d5/2 and d3/2 signal just one clear peak was detected, namely at 366.8 eV and 372.8 eV (Figure 6 A). The values are far away from the Ag and Ag_2O signals and can be attributed only to AgO [47], which reinforces the speculations and the indirect evidence brought up until now. Next, the sample containing 50% anatase and 50% rutile was analyzed (Ag/AgO-^{50}AA_^{50}AR) and it was expected that a considerable amount of Ag should be visible in the Ag3d XPS spectrum at 368.4 eV and 374.0 eV [48]. The expectations were fulfilled partially as 12.7% of the total silver species was metallic silver, while the rest was AgO. However, with the increase of the rutile content the amount of Ag increased gradually (0% - Ag/AgO-^{100}AA_^{0}AR, 7.2% - Ag/AgO-^{75}AA_^{25}AR, 12.7% - Ag/AgO-^{50}AA_^{50}AR and 15.1% - Ag/AgO-^{0}AA_^{100}AR). It should be mentioned that Ag nanoparticles are known to oxidize quite easily, therefore the original metallic silver content cannot be measured

accurately. Moreover, the sample without anatase contained 10.4% of Ag_2O (identified at 367.7 eV and 373.8 eV) [49] pointing out that a higher amount of Ag was present initially, while Ag_2O represents an intermediate step in the oxidation.

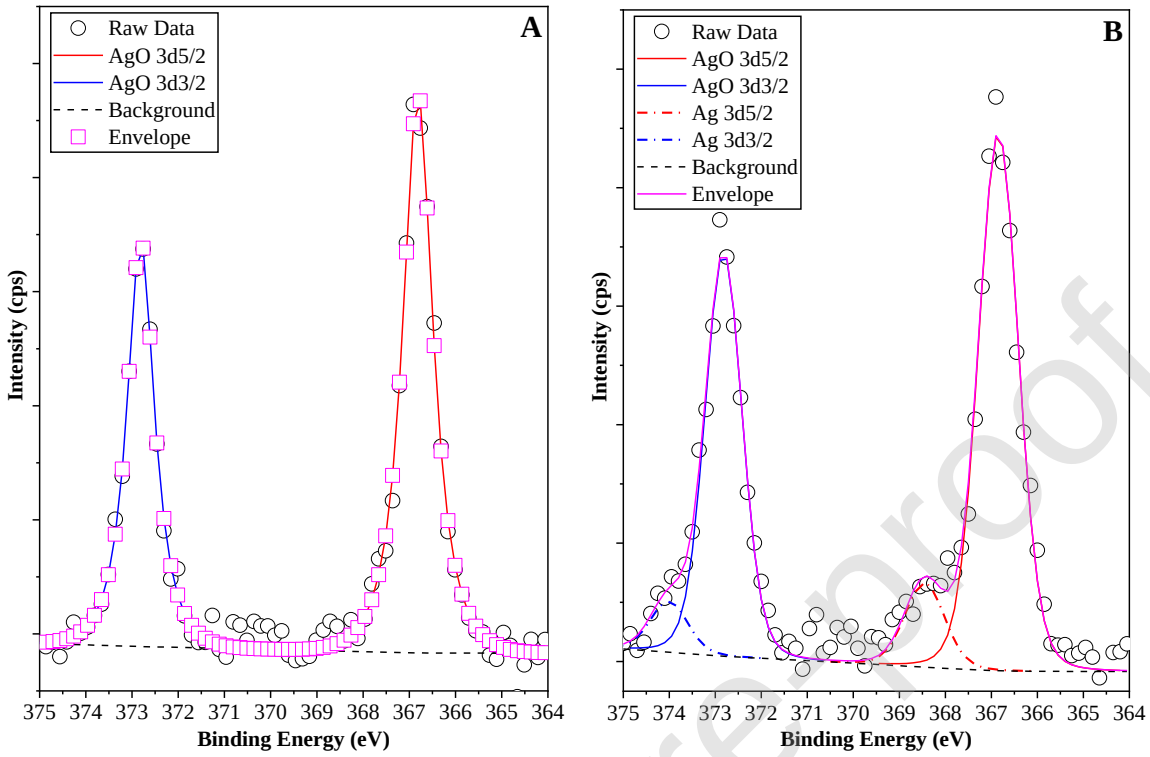

Figure 6: The Ag3d XPS spectra of the samples Ag/AgO-^{100}AA_^{0}AR (A) and Ag/AgO-^{50}AA-^{50}AR (B), demonstrating the presence of the two discussed species Ag and AgO, respectively. The envelope curve was represented by points (A) due to the overlapping of the spin-splitted signal components with the fitted main curve.

3.2. Effect of the noble metal-based nanoparticles on the photocatalytic activity of the titania

As can be seen in Fig. 6, the ^{0}AA_^{100}AR composites have the highest oxalic acid degradation yield (bare: 98.9 %; modified: 89.6 %, Fig. 7a), and ^{100}AA_^{0}AR samples have the highest activity in the degradation of phenol (bare: 60.6%, modified: 55 %, Fig. 7a). Interestingly, the commercial composites had higher activity than the modified TiO_2, when only one crystal phase was present. Sample Ag/AgO-^{75}AA_^{25}AR was an exception in the degradation of both phenol and oxalic acid, which was not surprising, as this sample was an exception also concerning its plasmonic band location at 357 nm (Fig. 1e) and it has the lowest indirect band gap energy (Fig. 4, 2.38 eV).

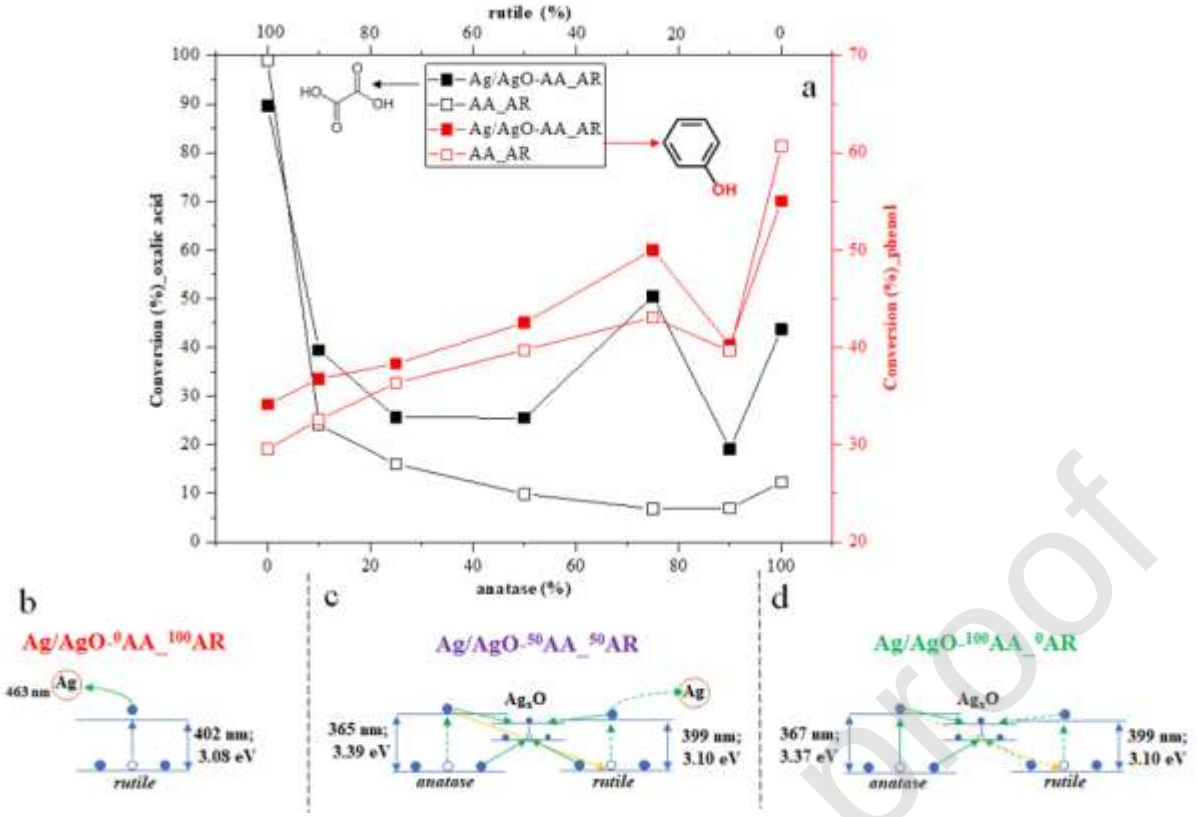

Figure 7. (a) Oxalic acid (black) and phenol (red) conversion on bare (hollow squares) and Ag/AgO modified (filled squares) photocatalysts; possible electron transfer mechanism on (b) Ag/AgO-^{0}AA_^{100}AR; (c) Ag/AgO-^{50}AA_^{50}AR; (d) Ag/AgO-^{100}AA_^{0}AR composites.

Based on Fig. 5, we found that by increasing the amount of anatase, the degradation yields would increase as well because anatase is generally considered a photocatalyst with higher yields, compared to rutile. This was proven in the case of phenol degradation but was not applicable in the case of oxalic acid, where the degradation yield decreases with the increase of the amount of anatase. It is well-known that during the usual photocatalytic degradation on the surface of titania-based materials, oxalic acid can adsorb quite well on the surface of the catalyst, while shows a much weaker affinity towards the surface of titania. The rutile phase is favorable compared to anatase because rutile can adsorb oxalic acid with higher efficiency than phenol [50]. Moreover, in the case of phenol degradation, sample ^{0}AA_^{100}AR had the lowest efficiency, because phenol adsorbs poorly. Presumably, in the case of rutile, adsorption/degradation of intermediates forming during phenol decomposition was favorable, while anatase adsorbs the intermediates with lower efficiency, degrading the phenol in the meantime with higher yield and making the surface available for radical generation and thus finally for phenol degradation. This statement can also be supported

because as the amount of the rutile increases in the samples, the amount of degraded oxalic acid is also increasing, while the concomitantly higher amount of anatase resulted in higher phenol degradation.

In order to explain the behavior of the composites, we have proposed an electron transfer mechanism for each composite system (Fig. 7 b-d).

(i) binary composite (Fig. 7b): in the case of Ag/AgO-^{0}AA_^{100}AR, the electron transfer occurs between the silver nanoparticle and rutile. This electron transfer has already been proven [43].

(ii) tertiary composite (Fig. 7d): in the case of Ag/AgO-^{100}AA_^{0}AR, the electron transfer is preferred between the anatase crystals and silver(II)-oxide particles, then between the rutile and anatase crystal phase, due to the low rutile content.

(iii) quaternary composite (Fig. 7c): silver nanoparticles transformed to Ag_xO with an increased amount of anatase (as shown in Fig. 5). In addition to the electron transfer between AgO and TiO_2 (suspected above, (ii)), an electron transition can also occur between anatase and rutile (in this case, the amount of the rutile is higher). The possibility of the anatase to interact with rutile is more tranquil than with Ag_xO, and due to that, the amount of the rutile is higher. Moreover, the Ag nanoparticles can accept the electrons from rutile (the electron will neutralize the generated hole in the rutile valance band from the anatase conduction band). Therefore, we can propose the existence of a quaternary composite, in which the electron from the anatase structure is "short-circuiting" another material, which resulted in low degradation yields.

The same mechanism could be applied in the case of other quaternary composites, where also the rutile-anatase electron transfer occurs. By increasing the amount of the anatase, the number of the electrons on the valance band is increasing. Therefore, it can be concluded that the chance that the electron is promoted from the conduction band of rutile to the conduction band of anatase is higher than the probability of the recombination on the rutile with the electron originating from the conduction band of anatase. Therefore, the number of holes necessary for the degradation of oxalic acid is not reached.

(iv) using the bare commercial TiO_2 composites, the anatase-rutile electron transfer could occur quickly, therefore they were able to degrade the model pollutants.

The supposed electron transfer mechanism can also be proven by using the degradation curve. For the degradation of oxalic acid, holes are needed, which has a preferred formation in this case, as shown in Fig. 7b, Ag nanoparticles accept the electrons from the conduction band of rutile, while in another case the hole traps an electron from anatase or Ag_xO. The

high degradation yield of phenol can be related to the amount of anatase since the anatase degraded phenol with higher efficiency than the rutile.

We can conclude that Ag nanoparticles enhanced the charge transfer on the surface of the titania if both crystal phases were present. Interestingly, if only rutile were present (^{0}AA_^{100}AR), the bare catalyst degraded efficiently oxalic acid compared to the modified TiO_2. Similarly, ^{100}AA_^{0}AR degraded phenol with higher yield comparing to the silver modified catalyst.

It is worth to mention that the activity of the catalysts was also investigated under visible light irradiation, but they have exhibited negligible activity (less than 8 %).

In order to understand the photocatalytic performance of the samples, photoluminescence measurements were carried out at an excitation wavelength of 325 nm. As can be seen in Fig. S2, with increasing rutile content, the characteristic emission band of TiO_2 showed a redshift (376 nm→385 nm) while the single band was split to a double peak, which is specific for the rutile based samples. With the deposition of the Ag nanoparticles, the band around 400 nm suffered a blueshift (except of sample Ag/AgO-^{75}AA_^{25}AR, which was unexpected, because it had one of the lowest plasmonic resonance band and the second-highest efficiency in the degradation for each model pollutant). We have also detected an enhancement in PL spectra in Ag_AgO_^{0}AA_^{100}AR and Ag_AgO_^{100}AA_^{0}AR samples, which could be attributed to the excitation of surface plasmons in Ag or AgO nanoparticles [51].

For a more in-depth investigation, we have deconvoluted the obtained PL spectra (Fig. S3). In the case of bare catalysts, we have found four different bands (376-385 nm; 411-423 nm; 461-467 nm; 513-521 nm), while in the case of modified catalysts five different peaks could be observed (375 nm; 392-411 nm; 418-433 nm; 467-470 nm; 513-528 nm). The first major difference between the modified and the bare catalysts is that the modified catalysts resulted in one more intensive response at the 392-411 nm region (second peaks). This band could be attributed to the presence of Ag/Ag_xO nanoparticles. Figs. S2, S3 shows the PL peak at ~375 nm (modified) and 376-385 nm (bare), which can be attributed to the presence of anatase (recombination of photoexcited electron-hole pairs) [52]. On the other hand, the peak around 375 nm cannot be observed in emission spectra of ^{0}AA_^{100}AR and Ag/AgO-^{0}AA_^{100}AR samples. Other bands were also observed, which were located at 411-433 nm, 461-470 nm, and 513-521 nm, which could be attributed to the shallow traps and oxygen vacancies [34].

As you can see in Fig. 8, a correlation between the PL measurements and phenol degradation was observed. Interestingly, the photoactivity increases with the increase of the photoluminescence of the 411-433 band. At first sight, it seems that these are contradictory results. However, if the luminescence signals' origin lies within recombination phenomena in traps, then the higher conversion of phenol is explainable. More precisely, if the charge traps are functioning correctly, some of the photogenerated electrons or holes can be trapped (and eventually neutralized by the other generated charge carrier pairs generated in the trap's vicinity), while its counterpart can freely migrate to the Ag-based components and generate reactive radical species, such as •OH and $•O^{2-}$.

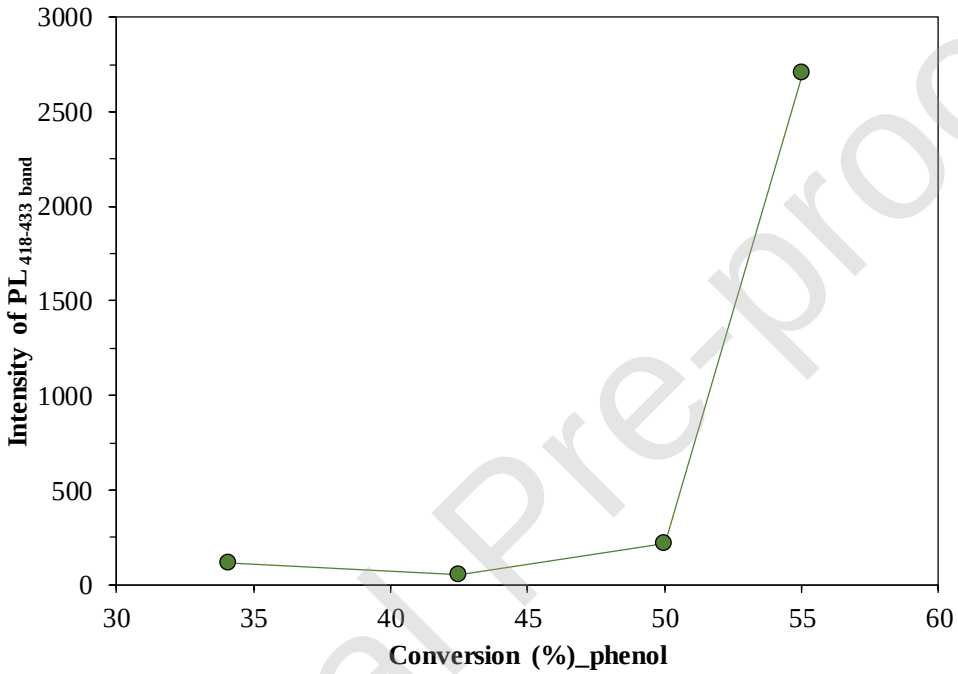

Figure 8. Correlation between the intensity of the 418-431 nm photoluminescence band with the conversion of phenol under UV irradiation.

3.3. Stability investigation of the samples

As it was already shown in the literature that the Ag-based materials can have stability and photocorrosion related issues [53], we examined the photocorrosion of the Ag nanoparticles with diffuse reflectance spectroscopy and with photodegradation tests in order to investigate the recyclability and long term stability of the samples.

3.3.1. Long term stability investigations

We have remeasured the diffuse reflectance spectra of the samples (after 6 months after the initial synthesis), to examine the possible transformation of silver nanoparticles into Ag_xO during the time.

In Table 1, we can observe the original value, which was obtained from the spectra measured after the synthesis processes and also the re-measured for value (after 6 months). We have remeasured the sample to figure out the possible transformation of the Ag nanoparticles. The "after the 2nd catalytic process" is the value of the samples, which are measured after the second degradation processes. In the first instance, we can assume that the silver nanoparticles have transformed into Ag_2O during the time (also discussed in the paragraph dealing with XPS results). The plasmonic band of Ag/AgO-^{0}AA_^{100}AR was initially located at 463 nm (Table 1), and after 6 months has and showed a redshift (to 475 nm, Table 1). Moreover, the band becomes narrower than the primary one.

The other samples (Ag/AgO-^{50}AA_^{50}AR; Ag/AgO-^{100}AA_^{0}AR) did not show any significant changes in their plasmonic band changes in time. Therefore, we can suppose that the content AgO is affected by any major aging process of six months.

Table 1. *The position of the plasmonic band maximum of the samples in different conditions.*

	Original (nm)	**Re-measured -*after 6 months*- (nm)**	**After the 2nd catalytic process**	
			oxalic acid (nm)	**phenol (nm)**
Ag/AgO-^{0}AA_^{100}AR	463	474	444	453
Ag/AgO-^{50}AA_^{50}AR	453	457	471	478
Ag/AgO-^{100}AA_^{0}AR	451	455	465	481

3.3.2. Recyclability of the samples

During the recyclability test of the samples, in the first instance, it was observed that the Ag/AgO-^{0}AA_^{100}AR sample's photoactivity was higher in the second cycle compared to the first one with 11 %, which confirmed the formation of Ag_2O in time, which re-transformed into Ag, enhancing the degradation of oxalic acid and phenol. In the case of oxalic acid, the Ag/AgO-^{50}AA_^{50}AR and Ag/AgO-^{100}AA_^{0}AR samples showed the same degradation yield in the second cycle. Since the position of the re-measured plasmonic resonance bands are the

same and there is no significant decrease/increase of the degradation yield in the second cycle, the small changes of the plasmonic resonance bands can be attributed to the agglomeration of Ag/Ag_xO nanoparticles. In the case of phenol, there is a minimal decrease in conversion value by using the Ag_AgO_^{100}AA_^{0}AR catalyst.

After the degradation processes, the plasmonic resonance bands showed a blue shift (oxalic acid – 444 nm; phenol- 453 nm, Table 1). The obtained plasmonic resonance bands have their maxima at a lower wavelength, which means that they have re-transformed to Ag nanoparticles. We suspected that this was possible by the reduction of Ag_xO by the photogenerated electrons. The plasmonic resonance bands of the Ag/AgO-^{50}AA_^{50}AR and Ag/AgO-^{100}AA_^{0}AR suffer a redshift, which could be attributed to the agglomeration of silver/silver-oxide nanoparticles [43, 44].

We can also conclude that the catalysts are not "deteriorated" during the catalytic processes, as the activity of the samples is unchanged or even higher in the second cycle (Figure 9).

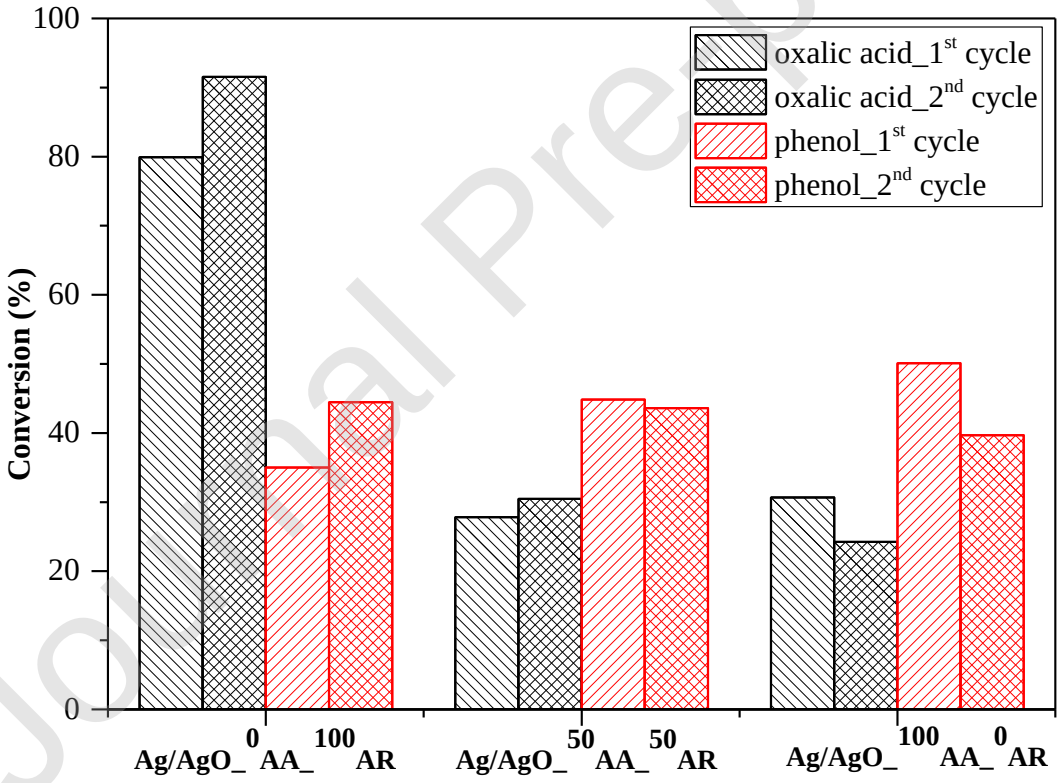

Figure 9. Recycling test on the Ag/AgO-^{0}AA_^{100}AR; Ag/AgO-^{50}AA_^{50}AR; Ag/AgO-^{100}AA_^{0}AR samples (black – oxalic acid, red- phenol)

4. Conclusions

As it was already known and predictable from the literature and our previous results, Ag nanoparticles were unstable and transformed into AgO nanoparticles, which process can be controlled by using different mixtures of commercial TiO_2 (Aldrich anatase (AA) and rutile (AR)). Ag nanoparticles can be deposited preferentially on rutile, while they could be transformed into other silver-based nanoparticles (Ag_xO) by increasing the amount of the anatase. Considering the results from DRS measurements, it can be affirmed that the Ag nanoparticles deposited on the surface of rutile can increase the efficiency of charge separation while on the surface of the anatase, the formed amorphous AgO nanoparticles are behaving similarly.

Regarding the photocatalytic efficiencies of oxalic acid, we can conclude that the rutile crystal phase is required for the sufficient degradation process. The photocatalytic efficiencies of the tertiary and quaternary composites were higher than those of the corresponding commercial TiO_2 mixtures. In the case of phenol degradation, anatase proved to be responsible for the degradation of the contaminant, while rutile can preferentially adsorb the intermediates during the degradation process.

After the aging process, the Ag nanoparticles deposited on the crytal phase of rutile were transformed into Ag_2O which have re-transformed to Ag nanoparticles after the degradation processes. On the other hand, the AgO on the surface of the anatase maintained its long term stability and the photocatalytic efficiency.

AUTHORSHIP STATEMENT

Manuscript title: Controlled formation of Ag-AgxO nanoparticles on the surface of commercial TiO_2 based composites for enhanced photocatalytic degradation of oxalic acid and phenol

All persons who meet authorship criteria are listed as authors, and all authors certify that they have participated sufficiently in the work to take public responsibility for the content, including participation in the concept, design, analysis, writing, or revision of the manuscript. Furthermore, each author certifies that this material or similar material has not been and will not be submitted to or published in any other publication before its appearance in the special issue of Catalysis Today

Authorship contributions:

Zsejke-Réka Tóth: writing the original draft, writing the review, validation, methodology, conceptualization

Klara Hernadi: supervision, funding acquisition

Lucian Baia: supervision, funding acquisition

Zsolt Pap: supervision, investigation, conceptualization

Gábor Kovács: writing the original draft, writing the review, methodology, investigation

All persons who have made substantial contributions to the work reported in the manuscript (e.g., technical help, writing and editing assistance, general support), but who do not meet the criteria for authorship, are named in the Acknowledgements and have given us their written permission to be named. If we have not included an Acknowledgements, then that indicates that we have not received substantial contributions from non-authors.

20.12.2019 The Authors

Declaration of interests

The authors declare that they have no known competing financial interests or personal relationships that could have appeared to influence the work reported in this paper.

Acknowledgments:

The research was carried out in the frame of GINOP-2.3.2-15-2016- 00013 and PN-III-P1.1-TE-2016-1588 projects. Zs. Pap expresses his gratitude towards the Hungarian Academy of Sciences, Premium Postdoctoral Fellowship project. G. Kovács acknowledges his financial support for NKFIH PD-125311 tender. Zs. Pap and G. Kovács acknowledge the financial support for the “Bolyai János” scholarship.

Special thanks to Bárdos Enikő, Milica Todea, and Monica Focsan for carrying out the TEM, XPS and PL measurements.

References

[1] D. Ficai, A. Ficai, E. Andronescu, 1 - Recent advances in using magnetic materials for environmental applications, in: A.M. Grumezescu (Ed.) Water Purification, Academic Press2017, pp. 1-32.
[2] A. Fujishima, K. Honda, Nature, 238 (1972) 37-38.
[3] K. Nakata, A. Fujishima, Journal of Photochemistry and Photobiology C: Photochemistry Reviews, 13 (2012) 169-189.
[4] V. Etacheri, C. Di Valentin, J. Schneider, D. Bahnemann, S.C. Pillai, Journal of Photochemistry and Photobiology C: Photochemistry Reviews, 25 (2015) 1-29.
[5] Y. Shi, J. Huang, G. Zeng, W. Cheng, J. Hu, J. Membr. Sci., 584 (2019) 364-392.
[6] M.V. Dozzi, E. Selli, Journal of Photochemistry and Photobiology C: Photochemistry Reviews, 14 (2013) 13-28.
[7] C. McManamon, J. O'Connell, P. Delaney, S. Rasappa, J.D. Holmes, M.A. Morris, J. Mol. Catal. A: Chem., 406 (2015) 51-57.
[8] N.O. Gopal, M.H. Basha, Ceramics International, 44 (2018) 22129-22134.
[9] Q. Quan, S. Xie, B. Weng, Y. Wang, Y.-J. Xu, 14 (2018) 1704531.
[10] C. Suwanchawalit, S. Wongnawa, P. Sriprang, P. Meanha, Ceramics International, 38 (2012) 5201-5207.
[11] A. Ayati, A. Ahmadpour, F.F. Bamoharram, B. Tanhaei, M. Mänttäri, M. Sillanpää, Chemosphere, 107 (2014) 163-174.
[12] L.-C. Pop, V. Dracopoulos, P. Lianos, Applied Surface Science, 333 (2015) 147-151.
[13] B. Gupta, A.A. Melvin, T. Matthews, S. Dash, A.K. Tyagi, Renewable and Sustainable Energy Reviews, 58 (2016) 1366-1375.
[14] M.R. Al-Mamun, S. Kader, M.S. Islam, M.Z.H. Khan, Journal of Environmental Chemical Engineering, 7 (2019) 103248.
[15] M.A. Lara, C. Jaramillo-Páez, J.A. Navío, P. Sánchez-Cid, M.C. Hidalgo, Catal. Today, 328 (2019) 142-148.
[16] C. Han, S.-H. Li, Z.-R. Tang, Y.-J. Xu, Chemical Science, 9 (2018) 8914-8922.
[17] M. Pirhashemi, A. Habibi-Yangjeh, S. Rahim Pouran, Journal of Industrial and Engineering Chemistry, 62 (2018) 1-25.
[18] H. Li, Z. Su, S. Hu, Y. Yan, Applied Catalysis B: Environmental, 207 (2017) 134-142.
[19] H. Li, T. Chen, Y. Wang, J. Tang, Y. Wang, Y. Sang, H. Liu, Chinese Journal of Catalysis, 38 (2017) 1063-1071.

[20] D. Vidyasagar, S.G. Ghugal, A. Kulkarni, P. Mishra, A.G. Shende, Jagannath, S.S. Umare, R. Sasikala, Applied Catalysis B: Environmental, 221 (2018) 339-348.
[21] Z. Li, P. Zhang, T. Shao, X. Li, Applied Catalysis B: Environmental, 125 (2012) 350-357.
[22] Z.-D. Meng, T. Ghosh, L. Zhu, J.-G. Choi, C.-Y. Park, W.-C. Oh, J. Mater. Chem., 22 (2012) 16127-16135.
[23] H. Tang, Y. Wang, D. Zhang, K. Wu, H. Huang, Journal of Materials Science: Materials in Electronics, 27 (2016).
[24] H. Daupor, S. Wongnawa, Applied Catalysis A: General, 473 (2014) 59-69.
[25] Z.-M. Yang, Y.-Y. Liu, L. Xu, G.-F. Huang, W.-Q. Huang, Materials Letters, 133 (2014) 139-142.
[26] J. Li, W. Fang, C. Yu, W. Zhou, L. zhu, Y. Xie, Applied Surface Science, 358 (2015) 46-56.
[27] H. Wang, J. Li, M. Zhou, Q. Guan, Z. Lu, P. Huo, Y. Yan, Journal of Industrial and Engineering Chemistry, 30 (2015) 64-70.
[28] D.H. Cui, Y.F. Zheng, X.C. Song, J. Alloys Compd., 701 (2017) 163-169.
[29] H. Hua, Y. Xi, Z. Zhao, X. Xie, C. Hu, H. Liu, Materials Letters, 91 (2013) 81-83.
[30] M. Xu, L. Han, S. Dong, ACS Applied Materials & Interfaces, 5 (2013) 12533-12540.
[31] G. Liu, G. Wang, Z. Hu, Y. Su, L. Zhao, Applied Surface Science, 465 (2019) 902-910.
[32] G. Wang, X. Ma, B. Huang, H. Cheng, Z. Wang, J. Zhan, X. Qin, X. Zhang, Y. Dai, J. Mater. Chem., 22 (2012) 21189-21194.
[33] M.B. Bouzourâa, Y. Battie, A. En Naciri, F. Araiedh, F. Ducos, N. Chaoui, Opt. Mater., 88 (2019) 282-288.
[34] J. Singh, S. Sharma, S. Sharma, R.C. Singh, Optik, 182 (2019) 538-547.
[35] #x00ED, C. az-Uribe, J. Viloria, L. Cervantes, W. Vallejo, K. Navarro, E. Romero, Qui, #x00F1, C. ones, 2018 (2018) 8.
[36] R. Zhou, S. Lin, H. Zong, T. Huang, F. Li, J. Pan, J. Cui, 2017 (2017) 9.
[37] M.K. Seery, R. George, P. Floris, S.C. Pillai, Journal of Photochemistry and Photobiology A: Chemistry, 189 (2007) 258-263.
[38] Z. Wei, M. Janczarek, M. Endo, C. Colbeau-Justin, B. Ohtani, E. Kowalska, Catal. Today, 310 (2018) 19-25.
[39] L. Gomathi Devi, R. Kavitha, Applied Surface Science, 360 (2016) 601-622.
[40] Z.-R. Tóth, G. Kovács, K. Hernádi, L. Baia, Z. Pap, Sep. Purif. Technol., 183 (2017) 216-225.

[41] J. Tauc, Materials Research Bulletin, 3 (1968) 37-46.
[42] V. Amendola, O.M. Bakr, F.J.P. Stellacci, 5 (2010) 85-97.
[43] L. Baia, M. Baia, W. Kiefer, J. Popp, S. Simon, Chemical Physics, 327 (2006) 63-69.
[44] L. Baia, D. Muresan, M. Baia, J. Popp, S. Simon, Vib. Spectrosc, 43 (2007) 313-318.
[45] S. Feng, M. Wang, Y. Zhou, P. Li, W. Tu, Z. Zou, APL Materials, 3 (2015) 104416.
[46] R. Quesada-Cabrera, C. Sotelo-Vazquez, J.C. Bear, J.A. Darr, I.P. Parkin, 1 (2014) 1400069.
[47] V.K. Kaushik, Journal of Electron Spectroscopy and Related Phenomena, 56 (1991) 273-277.
[48] M. Romand, M. Roubin, J.-P. Deloume, Journal of Solid State Chemistry, 25 (1978) 59-64.
[49] J.S. Hammond, S.W. Gaarenstroom, N. Winograd, Analytical Chemistry, 47 (2002) 2193-2199.
[50] M. Batzill, Energy & Environmental Science, 4 (2011) 3275-3286.
[51] J. Singh, K. Sahu, R. Singh, T. Som, R.K. Kotnala, S. Mohapatra, J. Alloys Compd., 786 (2019) 750-757.
[52] A. Aronne, M. Fantauzzi, C. Imparato, D. Atzei, L. De Stefano, G. D'Errico, F. Sannino, I. Rea, D. Pirozzi, B. Elsener, P. Pernice, A. Rossi, RSC Advances, 7 (2017) 2373-2381.
[53] B. Weng, M.-Y. Qi, C. Han, Z.-R. Tang, Y.-J. Xu, ACS Catalysis, 9 (2019) 4642-4687.